Food Chemistry 332 (2020) 127150

Contents lists available at ScienceDirect

Food Chemistry

journal homepage: www.elsevier.com/locate/foodchem

Simple and selective optical biosensor using Ultrasonicator synthesis of 5-((anthracen-9-ylmethylene) amino)-2,3-dihydrophthalazine-1,4-dione for direct detection of ascorbic acid in vegetables and fruits

Shenbagavalli Kathiravan[a], Ellairaja Sundaram[d], Bella Antony Paulraj[b], Princy Merlin Johnson[b], Sheng-Tung Huang[c], Veerappan Mani[c], Vairathevar Sivasamy Vasantha[a,*]

[a] Department of Natural Products Chemistry, School of Chemistry, Madurai Kamaraj University, Madurai 625 021, Tamil Nadu, India
[b] PG and Research Department of Chemistry, Bishop Heber College, Tiruchirappalli 620017, Tamil Nadu, India
[c] Department of Chemical Engineering and Biotechnology, National Taipei University of Technology, No.1, Sec. 3, Chung–Hsiao East Road, Taipei 106, Taiwan
[d] Department of Chemistry, Vivekananda College Tiruvedakam West, Madurai 625 234, Tamil Nadu, India

ARTICLE INFO

Keywords:
Ultrasonication
Ascorbic acid
Imine
FRET mechanism
Optical biosensor
Density Functional Theory
Vegetables and Fruits

ABSTRACT

We report an optical biosensor using imine, 5-((anthrcene-9-ylmethylene) amino)-2,3dihydrophthalazine) 1–4-dione (ADD) for direct detection of ascorbic acid (AA) via FRET quenched. The ADD was successfully prepared by using simple ultra - sonication method, which was characterized by various spectroscopic techniques. The fluorescence intensity of ADD probe was drastically quenched in presence of AA, and shown excellent selectivity towards the detection of AA in presence of possible biological active interferences. A wide linear range from 0.25 to 190 μM was achieved towards the detection of AA with a LOD of 10 nM. The occurrence of FRET mechanism is due to intermolecular hydrogen bonding between ADD and AA, which was confirmed by Density Functional Theory calculations. Moreover, the biosensor was successfully applied for the detection of AA in real samples such as fruits and vegetables to demonstrate the practicability. In addition, the developed biosensor could be a simple and economically cheap platform for the detection of AA in food samples.

1. Introduction

Vitamin C, chemically known as ascorbic acid (AA) is acting as a strong reducing agent, coenzyme and essential nutritional factor production of certain neurotransmitters. AA is naturally occurring antioxidant and playing central roles in many biological processes inside the human body (Na, Qu, Chen, & Su, 2018). Also, AA protects us against immune system deficiencies, cardio vascular disease, helps to from collagen in bones and absorbs irons and finally helps the nervous system by converting amino acids into neurotransmitters (Biswas, Pal, Kumar, & Koner, 2018). It is classified as an essential antioxidant for the human body. Due to its antioxidant properties, AA is widely used in food, animal feed, beverages, cosmetics, and pharmaceutical formulations (Astray et al., 2009; Liu et al., 2016). The RDA (Recommended Daily Allowance) and Nutrition Board under the Institute of Medicine of the National Academies has suggested 75 mg/day for female and 90 mg/day for male (Fong, Chin, & Ng, 2016). The normal and healthy range of AA in human blood plasma is 61–80 μM (H. Liu, Na, Liu, Chen, & Su, 2017). As human body unable to synthesize AA, it should be taken through our nutrition (He & Zhang, 2017). AA deficiency in the nutrition causes several health disorders such as, fatigue, scurvy, feelings of weakness, bruising easily, bleeding of the gums, pain in the joints and iron deficiency (anemia), whereas abnormal AA levels leading to different kind of diseases like Diarrhea, Heartburn, Dizziness, Dehydration etc (Rao et al., 2017).

As far as literature survey concerned, plenty of analytical methods have been developed for the detection of AA, such as electrochemical sensors (Badea et al., 2018; He, Li, Zhang, & Luo, 2017), titration methods (Elgailani et al., 2017), spectrophotometry (Bushway, King, Perkins, & Krishnan, 1988), chromatography (El-Din, 2012), chemiluminescence (Hasanin & Fujiwara, 2018; Zhu et al., 2016), and enzymology capillary electrophoresis (Tortajada-Genaro, 2012). Many of these techniques are bulky, expensive, depend on tedious sample preparation, and time consuming (Gualandi et al., 2018; Liu & Pang, 2018).

For example, HPLC based reversed-phase liquid chromatographic method has been reported for the simultaneous determination of AA (ASC) and salicylamide (SAL) in their combined dosage form by using

* Corresponding author.
E-mail addresses: vasantham999@yahoo.co.in, sivarunjan@gmail.com (V.S. Vasantha).

https://doi.org/10.1016/j.foodchem.2020.127150
Received 3 December 2019; Received in revised form 23 May 2020; Accepted 24 May 2020
Available online 28 May 2020
0308-8146/

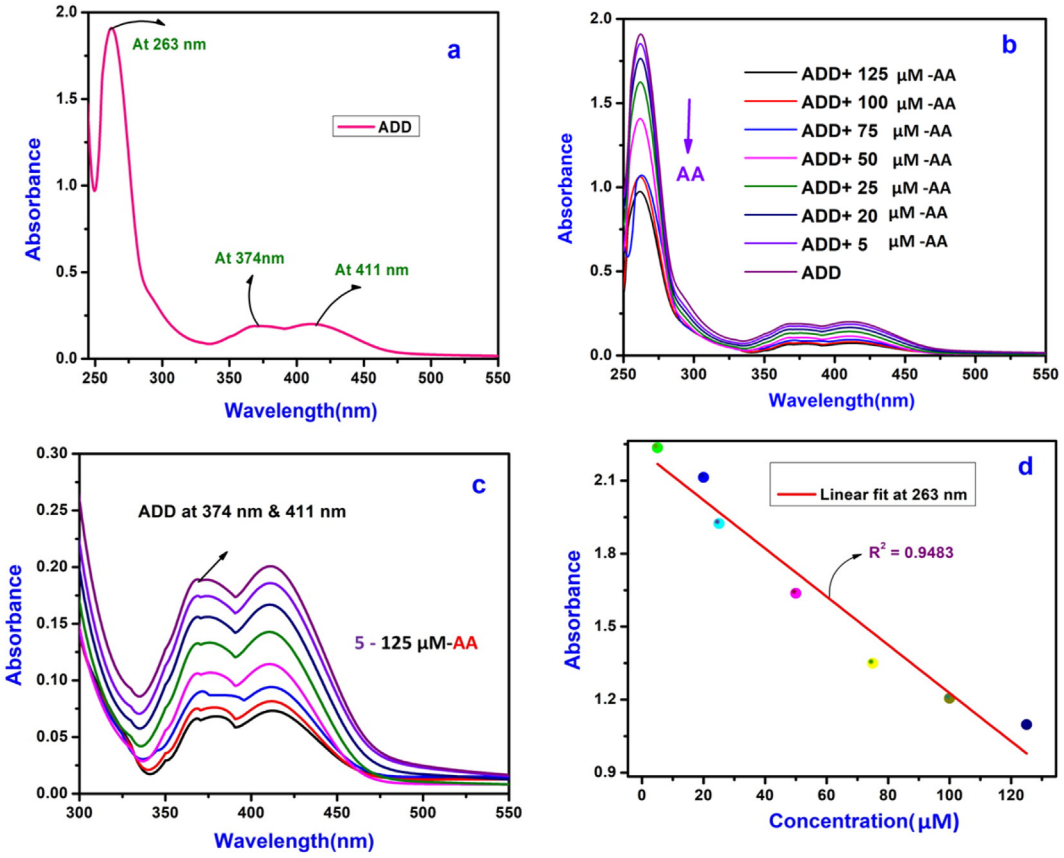

Fig. 1. (a) UV–Vis spectra of ADD, (b) UV–Vis spectra of for different concentrations of AA from 0 μM to125 μM, (c) Enlarged UV–Vis spectra ADD in presence of AA at 374 nm & 411 nm. (d) linear spectra at 263 nm: Absorbance vs. [AA] (μM), here the concentration of ADD is 2.5 × 10^{-5} M in phosphate buffer pH = 7.4.

CLC Shim-pack C8 column (250 × 4.6 mm, 5 μm particle size) over a concentration range of 0.50–10.00 and 5.00–50.00 μg mL^{-1} for ASC and SAL, respectively with limits of detection (LOD) of 0.048 and 0.676 μg mL^{-1} (El-Din, 2012). However, much simpler electrochemical AA sensors have been developed using, conducting polymer (X. Liu et al., 2014), nanomaterial's (Su, Sun, & Liao, 2017; Zhu, 2017) and quantum dots (Gai et al., 2013). Recently, an organic based electrochemical transistor sensor (OECT) with a molecularly imprinted polymer (MIP)-modified gate electrode was prepared for the detection of AA with the linear range from 1 to 100 μM and low detection limit of 10 nM and a sensitivity of 75.3 μA (Zhang et al., 2018). In another aspect, an electrochemical sensor for the simultaneous determination of uric acid (UA), dopamine (DA), AA and NO^{2-} have been developed with LOD of 11 nM, 30 nM, 41 nM, and 18 nM, respectively (Tukimin, Abdullah, & Sulaiman, 2018). Newly a bimodal electrochemiluminescence system based sensor has been reported using graphitic carbon nitride quantum dots (g-CNQDs) for the detection of AA from 3.5 to 330 nM, with LOD of 110 pM (Wang et al., 2018). Recently, another chemiluminescence based AA sensor has been reported based on ultrathin cobalt oxyhydroxide (CoOOH) nanosheets, which displayed the linear range of 1–500 pmol L^{-1} and LOD of 39 fmol L^{-1} (Xu et al., 2018).

Similarly, there are numerous optical sensors using graphene quantum dots (GQDs) are reported for the detection of AA. HRP enzyme based fluorescent sensor has been reported using H_2O_2, catechol and GQDs based on the fluorescence quenching for the detection for AA within the linear range from 1.11 to 300 μM and LOD of 0.32 μM (Liu et al., 2017). A GQDs-Cu^{2+} modulated dual-functional fluorescent probe was developed for the detection of AA with linear range from 0 to 12 μmol L^{-1} and LODs of 20.3 nM (Na et al., 2018). Another group reported CdSe@SiO_2@CdTe quantum dot hybrid as an ultrasensitive green fluorescence probe for the detection of AA from 0.1 to 5.0 μM, within the LOD of 35 nM (J. Wang, et al., 2017). A dual mode sensor using B, N, S co-doped carbon dots was applied for the detection of AA using the conjugated, BNS-CDs@Fe^{3+}, was demonstrated for AA sensing with a good linear range from 0.1 to 600 μM along with low LOD of 0.05 μM (Liu et al., 2018). FRET mechanism based sensor has also been reported for AA using GQDs and squaric acid (SQA)-iron (III). Recently, a fluorogenic probe, 4-azido-7-nitrobenzo-2-oxa-1, 3-diazole (NBDN3), has been developed for multiple detection of AA, cysteine and homocysteine (Biswas et al., 2018). Although,variety of GQDs based optical sensors have been reported for AA, they encounter several drawbacks, such as high-temperature requirement for the GQDs synthesis, low yield of GQDs, low quantum yield, tedious mechanism prediction during sensing, size effect, difficult of the surface modification, low photostability and high-cost preparation methods.

Besides, GQDs based sensors are lacking desirable linear range and LOD, for the detection of AA. Because a reliable sensor should cover both normal as well as diseased range of any analyte as prescribed by the various health organizations. Recently, fluorescent based optical sensors have been playing an alternating analytical tool to detect the various metal ions (Wu et al., 2017), anions (Dey, Al Kobaisi, & Bhosale, 2018), biomolecules (Zhang, Wang, & Lv, 2018) etc. Recently, numerous fluorimetric optical biosensors (Girigoswami & Akhtar, 2019) and immunosensors (Klos-Witkowska, 2016) have been developed for many biomolcule because of their attractive analytical characters such as, amplified sensitivity, selectivity, low-cost and practical feasibility (Ellairaja, Shenbagavalli, Ponmariappan, & Vasantha, 2017).

Based on the detailed literature survey on fluorescent-based sensors, it is clearly revealed that almost all the reports have utilized quantum dots alone or enzyme as sensing elements for AA detection. Further, most of the reports have used a tedious protocol for the synthesis of

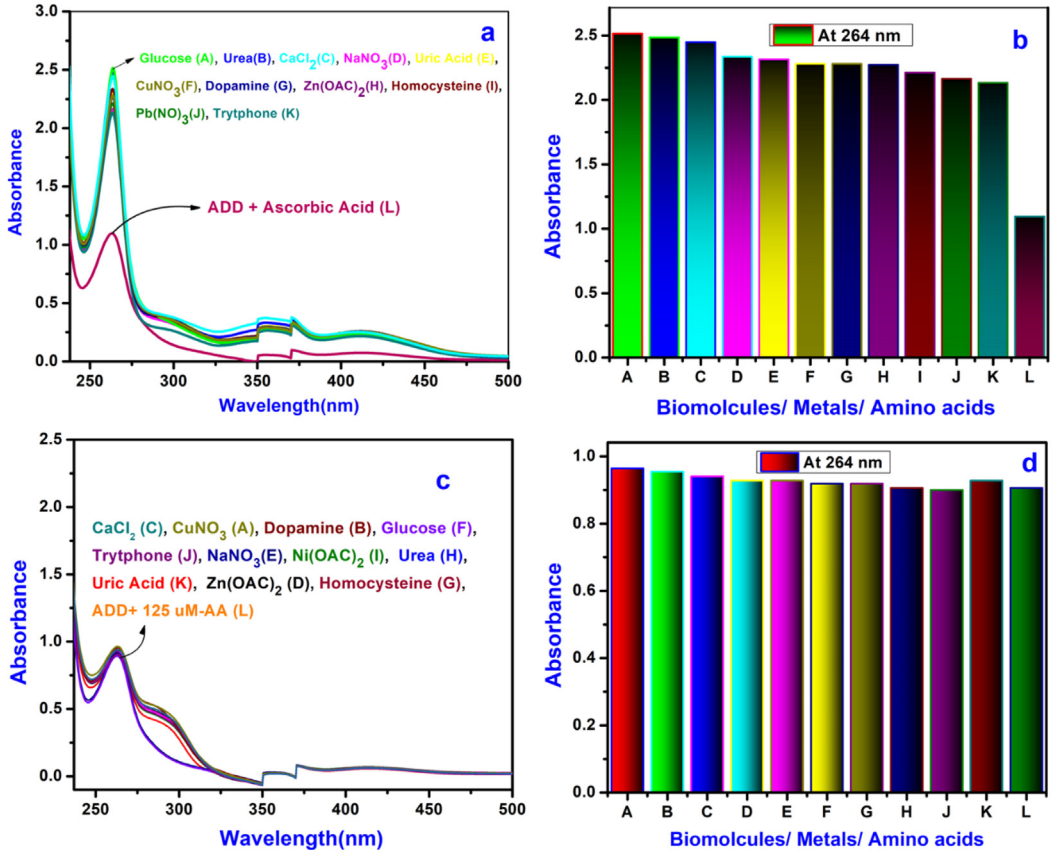

Fig. 2. (a) Selectivity studies of ADD in presence of other interfering of biomolecules and metals ions(b) Corresponding bar diagram for the selectivity studies. (c) Competitive studies of ADD in presence of higher concentration of other potential molecules and the corresponding bar diagram (d). The concentration of ADD was maintained as 2.5 × 10^{-5} M, and the concentration of interfering compounds was 1 × 10^{-3} M, prepared in phosphate buffer pH 7.4.

quantum dots (Ankireddy & Kim, 2015) and costely enzymes (Csiff Ary et al., 2016). Recently in our group,using a simple ultrasonication method for synthesis of fluroscence based simple imine moiety. Its main advantages are fast synthesis, low cast and using less solvent, compare to above methods like as reflux and doping methods. However, only one reports are available based on fluorophore optical sensor for AA quantification without reporting for the low detection limit, interference and linear sensing range of the sensors (Biswas et al., 2018). Hence, we synthesized a novel fluorophore ADD using greener synthetical protocol and developed fluorescent sensor with high excellent selectivity and sensitivity for direct detection AA in presence of all other interferences. Since there is no optical sensor for direct detection of AA reported so far, we have developed a simple sensor for the direct of AA which has linear range of detection in the normal and diseased range of AA from 0.25 to 190 μM with the LOD of 10 nM. Further, our biosensor has been applied to detect AA in different types of fruits and vegetables.

2. Materials and methods

Chemicals used such as 9-Anthracenealdehyde, luminol, glacial acetic acid, HPLC grade ethanol, ascorbic Acid, bilirubin, uric acid, urea, creatinine, creatine, L-dopamine, D-glucose, and various acetate salts of metal ions (Zn^{2+}, Cd^{2+}, Ca^{2+}, Ag^{+}, Na^{+}, K^{+}, Fe^{2+}, Fe^{3+}, Co^{2+}, and Cu^{2+}) were purchased from Sigma and used as such. Sodium dihydrogen phosphate (NaH_2PO_4), disodium hydrogen phosphate (Na_2HPO_4) and sodium phosphate (Na_3PO_4) were purchased from CDH fine chemicals India.

^{1}H and ^{13}C NMR analysis were performed using $CDCl_3$ and DMSO-d_6 as solvents containing a trace quantity of tetramethylsilane (TMS) as internal standard using Bruker-500 MHz spectrometer from CECRI, Karaikudi and chemical shifts were reported in ppm at 25 °C. Mass spectra and UV spectra were recorded using JASCO-390 the double beam UV − Vis spectrophotometer. Fluorescent measurements were done by HORIBA JOBINYVON spectrophotometer having a detector S (SCD3) in 350 nm- 700 nm.

2.1. Synthesis of 5-((anthrcene-9-ylmethylene) amino)-2, 3dihydrophthalazine) 1–4-dione: (ADD)

A greener, rapid, and simple synthetic approach based on ultra-sonication method was adopted to synthesis the fluorescent probe (ADD). Briefly, 9-anthracenealdehyde (1.0 g, 1 equi.) and luminol (0.85 g, 1equi) were dissolved in 10 mL of absolute ethanol. Then, 0.5 mL of glacial acetic acid was added into the solution as a catalyst. The slightly light yellow color and then was sonicated for 30 mins. Then, finally a dark-yellow colored solution was obtained. The resulting solution was allowed to cool at room temperature and finally a yellow colored precipitate was formed. The crude product was washed twice with absolute ethanol and diethyl ether and then dried over $MgSO_4$ under vacuum. The purity of the product was confirmed by using thin layer chromatography by observing the appearance of single spot. The needle shape product was formed. The yield was calculated as 0.72 g (95%). Moreover, this is the first imine based fluorescent probe synthesized for the detection AA.

2.2. ESI-MASS, NMR and IR data for the synthesized ADD

^{1}H NMR (400 MHz, DMSO) δ 8.97 (s, 1H), 8.71 (s, 1H), 6.56 – 6.46 (m, 3H), 5.71 (d, J = 8.3 Hz, 2H), 5.25 (dd, J = 11.1, 4.3 Hz, 2H), 5.16 – 5.09 (m, 2H), 4.95 (t, J = 7.9 Hz, 2H), 4.82 (s, 2H), 4.45 (d,

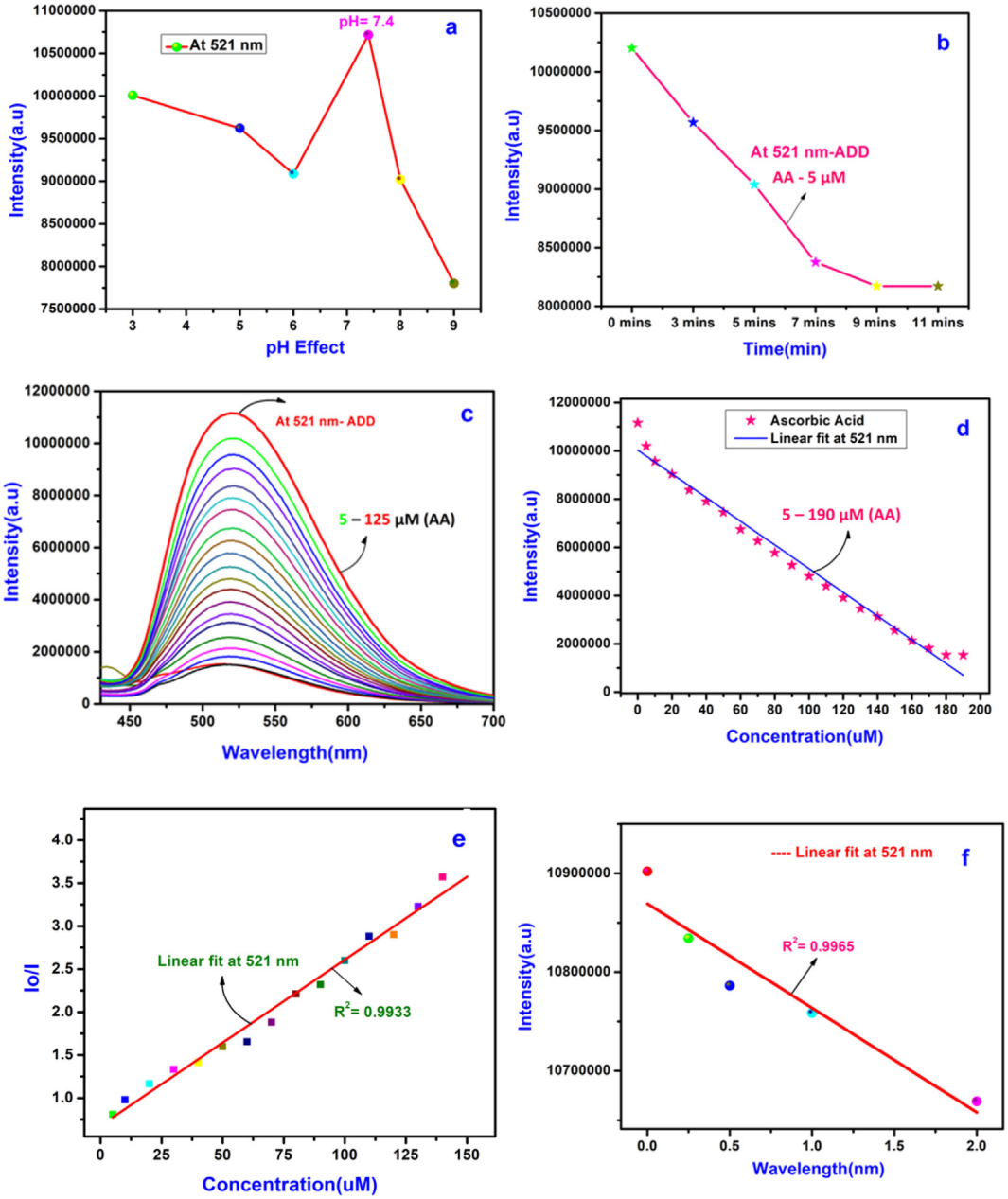

Fig. 3. (a) Effect of different pHs in fluorescent property of ADD molecule (b) Optimization of quenching time during the interaction between ADD and AA based on emission changes t (c) Emission spectra of ADD while varying the concentration of AA from 5 µM to190 µM. (d) Corresponding linear plot drawn in error bars 5%. (e) Corresponding stern volmer linear plot (f) Corresponding LOD calculations of linear plot 3Sa/b and error bars 5%. [Concentrations of ADD is 2.5 × 10–5 M, and ascorbic acid 5 µL, 500 × 10–6 M, in pH 7.4, phosphate buffer.].

J = 7.5 Hz, 1H), 4.39 (d, J = 8.1 Hz, 1H) ppm. ^{13}C NMR (75 MHz, DMSO) δ 193.02, 160.22, 150.32, 149.55, 134.07, 132.72, 130.21, 129.51, 128.19, 128.11, 125.45, 124.68, 123.27, 122.32, 115.29, 109.37, 108.32. Observed mass $[M + H]^+$ = 367.15. IR Spectra for ADD fluorophore 1659 cm^{-1} (Strong), 3019 cm^{-1}, 1600 cm^{-1} and 680–860 cm^{-1} peaks are corresponding to –CH═N– stretching, –NH- stretching secondary amine, –C═O– symmetric stretching and aromatic –CH– bending vibrations, respectively of ADD.IR Spectra ADD + AA for 1661 cm^{-1} (strong), 1757 cm^{-1}, 3022 cm^{-1}, 3417 cm^{-1} & 3318 cm^{-1} and 680–860 cm^{-1} peaks are corresponding to –CH═N– stretching, –CO–O– symmetric stretching frequency, –OH– stretching vibration in broad intermolecular bonded, –NH– stretching secondary amine, and aromatic –CH– bending vibrations, respectively of ADD + AA (Figs. S1–S4).

2.3. The procedure for detection of AA using ADD probe by UV–Vis and fluorescent methods

i) UV–Vis method: 2 mL of buffer solutions (pH 7.4), 50 µL of 1 × 10^{-3} ADD solution and 5 µM concentration AA were mixed, shaken thoroughly, and kept for 2 mins. Subsequently, the UV–Vis spectra was recorded and for the detection of AA.

ii) Fluorescent method: At room temperature, 1 mL of 0.1 M buffer solution (pH 7.4,), 20 µL of 1 × 10^{-3} M ADD solution, and 5 µM concentration of AA were added. The mixture was shaken thoroughly and kept aside for 5–10 min afterwards, the fluorescence spectra were recorded in the range of 430–700 nm with an excitation wavelength of 405 nm. The slit widths of excitation and emission were 5 nm. The maximum fluorescence intensity was used for the quantitative analysis of AA.

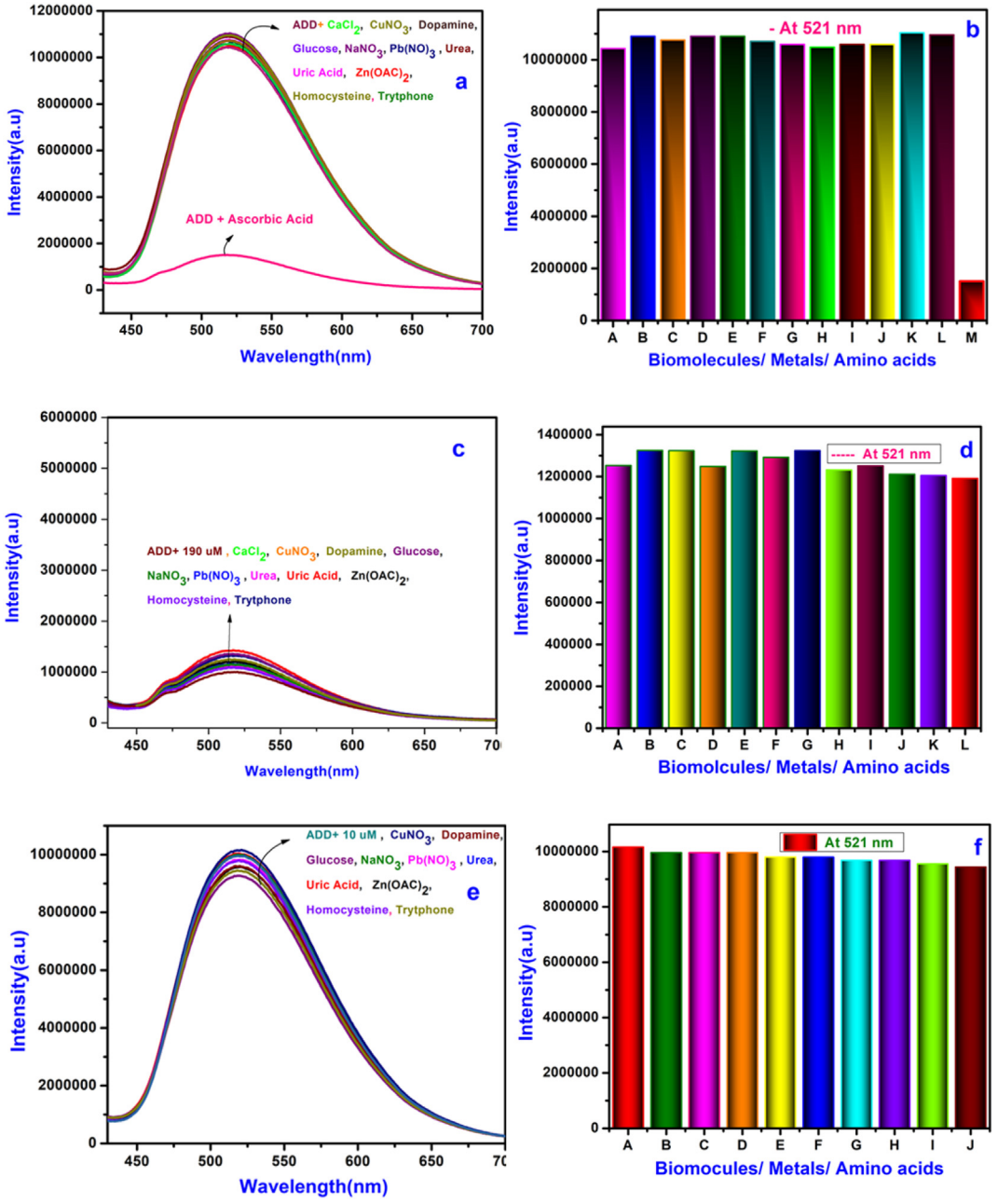

Fig. 4. (a) Emission spectra of ADD for selective detection of AA in presence of interfering biomolecules and metals ions. (b) Corresponding bar diagram based on change in emission. (c) Competitive studies of ADD in presence of other interferents at lower (5 μM) and higher (190 μM) concentrations (e) of AA diagram (d) Corresponding bar profile for lower and higher concentration (f) ranges of AA [The concentration of ADD is 2×10^{-5} M pH 7.4, phosphate buffer, and other interferents is concentration of 0.001 M]

3. Result and discussion

3.1. Photo physical properties of ADD

Under optimized conditions, a UV–Visible spectrum of ADD was recorded in pH 7.4 buffer. And it has shown three peaks at 263 nm, 374 nm and 411 nm, respectively in which the peak at 263 nm is due to π-π* transition and peaks at 374 nm and 411 nm are due to n- π* transitions. While adding various concentrations of AA from 0 to 125 μM, a TURN OFF responses were observed in the peak at 263 374 nm and 411 nm. However the decreased in the intensity was observed in the at peak 263 nm. And hence the linear range was recorded only at 263 nm. all corresponding figure are shown in (Fig. 1a - d).

3.2. Selectivity and competitive behavior of ADD

At optimized conditions, the selective nature of the synthesized ADD for AA was tested in presence of other possible biological interfering species such as, DA, glucose, urea, UA, homocysteine, and tryptophan and metal ions like, Ca^{2+}, Cu^{2+}, Na^{+}, Ni^{2+}, Pb^{2+}, and Zn^{2+}. For all the tested interfering species, the absorption of the peak at 263 nm is increased slightly. based on the results observed in Fig. 2a and b, we can firmly say that our ADD is highly selective for AA irrespective of the coexistence of other potential interfering molecules. To further support the selective nature of our ADD, we have performed competitive experiments as well. Because our human bio fluids consists of all type of biomolecules and metal ions, so it is necessary to analysis the competitive response of ADD in presence of other interferents along with AA.

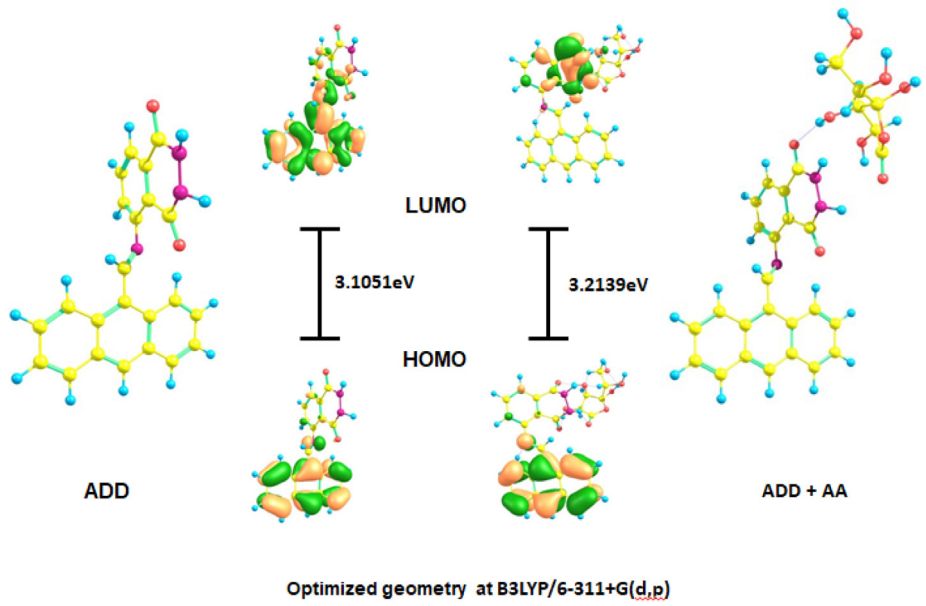

Fig. 5. DFT studies of the fluorophore ADD.

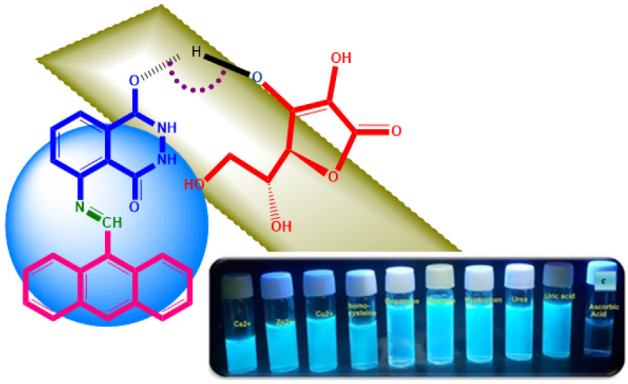

Scheme 1. Schematic representation of hydrogen bonding formation between ADD and AA during interactions., visible image in colour of ADD, the presence of different biomolecules. in AA inside UV chamber.

In detail, to one equivalent of ADD in 2.5 × 10^{-5} M and AA (500 μL in 500 × 10^{-6} M) in pH 7.4 buffer, one equivalent of other interferents (50 μL, 1 × 10^{-3} M) were added one by one. The corresponding absorbance changes (Fig. 2c and d) at 263 nm, 374 nm and 411 nm were observed and results have shown that only a negligible changes were observed even at higher concentration ranges of all interferents. Hence, our synthesized ADD is highly selective and shown a very good competitive nature in presence of all interferents.

3.3. Fluorescent response of ADD in different pH

The pH effect on emission spectra of ADD was examined in different pHs. In the pH range from 3 to 6, a decrease in intensity of ADD was observed which may be probably due to protonation, however, at pH 7.4, there was a sudden increase in the intensity. This must be due to existence of ADD in neutral form. On further increase of pH, there is sharp decrease in emission intensity due to deportation. So, finally, pH 7.4 is selected as optimum for UV–visible and emission studies (Fig. 3a) (Fig. S5).

3.4. Fluorescent response of ADD towards the detection of AA

The fluorescent response of the ADD was studied in detail. Under optimized concentration, ADD has shown a sharp and intense fluorescence peak at 521 nm (Fig. 3c and d). While adding the AA, the intensity of ADD at 521 nm was gradually quenched. As shown in Fig. 3b maximum quenching was observed at 10 min for all concentrations of AA (Fig. 3b). The linear range was found from 5 μM to 190 μM with the LOD of 10 nM. The quenching of ADD by AA was further supported by Stern Volmer quenching constant and quenching efficiency. The quenching constant (K_{sv}) and the quenching efficiency as calculated as 1.7491 × 10^{8} M and 53%, respectively and the corresponding limit of detection (LOD) calculated by linear plot using the standard formula 3Sa/b (Fig. 3e and f).

3.5. Selective and competitive analysis based on emission changes

The selectivity and competitive properties of AA were tested based on the fluorescent intensity change. Interestingly, the fluorescence studies revealed that the probe has shown high response for AA even in the presence of all the interferents. Firstly, the fluorescence response of the ADD towards (A), urea (B), uric acid (C), glucose (D), DA (E), Tryptophan (F), and homocysteine (G), and also metal ions like Zn^{2+} (H), Pb^{2+} (I), Ca^{2+} (J), Na^{+} (K), Cu^{2+} (L), and ADD + AA (M) was tested. The results are represented as a bar diagram. Except AA, remaining biomolecules and metal ions have shown a negligible TURN-ON fluorescence changes. But, presence of AA the fluorescent intensity of ADD was quenched obviously at 521 nm. This was further evinced by analyzing the competitive behavior of ADD in presence of the aforementioned interfering species (Fig. 4a & 4b). Competitive studies were performed at both lower (5 μM) and higher concentrations (190 μM) of AA, while constant high concentration (1 × 10^{-3} M) was maintained for the other species. In detail, to one equivalent of ADD (50 μL, in 2.5 × 10^{-5}M), one equivalent of AA (5 μM, 500 × 10^{-3} M in pH 7.4 buffer) and other interferents like Cu^{2+} (A), ADD + 5 μM AA (B), urea (C), UA (D), DA (E), glucose (F), Na^{+} (G), Zn^{2+} (H), tryptophan (I), homocysteine (J) and Pb^{2+} (K) biomolecules, metal ions like and were added one by one and the corresponding bar diagram emission profile was noted at 521 nm (Fig. 4e & 4f). This same protocol was repeated for higher concentration (190 μM) of AA and other interferents like corresponding of Zn^{2+} (A), DA (B), Urea (C), UA (D), Glucose (E), homocysteine (F), and tryptophan (G) and metal ions like Na^{+} (H), Pb^{2+} (I), ADD + 190 μM AA (J) and Cu^{2+} (K) the corresponding bar diagram of fluorescence spectra were analyzed (Fig. 4c & 4d). Our

Table 1
Analysis of AA in real samples.

Real Sample	[a]Dilution	[b]Found (μM)	[c]Spiked (μM)	[d]Intensity (a.u)	Recovery (%)
Banana	10	42 μM	85 μM	4,778,120	95
			100 μM	3,059,460	102
Chives	20	10 μM	100 μM	4,396,690	91
			140 μM	2,558,360	86
Garlic	105	5 μM	30 μM	8,375,780	110
			50 μM	7,103,130	103
			80 μM	5,521,930	104
Guava	20	30 μM	40 μM	6,068,100	97
			60 μM	5,137,050	98
			120 μM	3,837,750	98
Kiwi	55	20 μM	50 μM	6,267,530	101
			130 μM	2,558,360	97
Onion	55	10 μM	10 μM	9,037,930	102
			60 μM	6,267,530	99
			110 μM	3,916,100	101
Red Chilly	115	75 μM	35 μM	4,396,690	94
			75 μM	2,558,360	100
Green Chilly	25	8 μM	40 μM	7,458,110	101
			80 μM	5,264,520	99
			110 μM	3,916,100	99
			120 μM	3,457,840	98
Grape Fruit	15	15 μM	55 μM	6,267,530	100
			125 μM	3,126,960	105
			165 μM	1,536,120	102
Spinach	60	40 μM	5 μM	3,457,840	99
			35 μM	2,558,360	98
Tomato	25	30 μM	95 μM	4,803,100	103
			115 μM	3,916,100	95
Papaya	105	5 μM	15 μM	9,037,930	103
			25 μM	8,375,780	100
			95 μM	4,803,100	99
Potato	25	10 μM	10 μM	9,037,930	102
			50 μM	6,748,150	102
			70 μM	5,779,340	100
			150 μM	2,134,330	99
Lemon	10	5 μM	20 μM	8,706,855	100
			55 μM	6,767,530	105
Cabbage	15	70 μM	75 μM	3,126,960	105
			110 μM	1,536,120	102
Orange	7	5 μM	5 μM	9,568,970	100
			25 μM	8,375,780	99
			125 μM	3,457,840	97
Radish	50	3 μM	52 μM	6,023,435	98
			112 μM	4,156,395	99
			127 μM	3,457,840	103
			167 μM	1,824,310	102

Note: a = Dilution factor of real samples; b = The determination of unknown concentration of Crude sample in linear plot (μM); c = Spiked the known different concentration of Ascorbic acid in crude sample (μM); d = Intensity Overall concentration of actual intensity of Ascorbic acid (a.u).

studies were revealed that the ADD probe is highly selective and is shown very excellent competitive behavior in presence of other interferents.

3.6. DFT-TDDFT studies

In order to support the charge transfer mechanism between ADD and AA, DFT calculations were performed at the B3LYP/6-31 + G(d,p) and 6-311 + G(d,p) levels by using Gaussian 09 software program (M.J, G.W, B, E, M.A., R, et al., 2010). The corresponding energy level diagram is shown in (Fig. 5**).** The geometries of ADD and ADD + AA were optimized using the above-mentioned basis sets. Frontier molecular orbital analysis (FMO) of ADD reveals that the HOMO is majorly spread over the anthracene unit, then little contribution to imine group. The LUMO is spread from the anthracene to imine group predominantly with an energy difference of 3.1051 eV. After binding with the AA, there was no change in the HOMO and it was once again localized on anthracene moiety and imine group. But in LUMO the electron charge density was transferred to from imine to the luminol-AA joined group with the energy difference of 3.2139 eV. This slight increase in HOMO-LUMO energy gap (0.11 eV) of ADD + AA might be due to the binding of AA with ADD through hydrogen bonding.

3.7. Plausible mechanism for the biosensor

Based on the emission and DFT data, it is clearly understood that, the probe has shown an intense emission peak at 521 nm, which may be due to the occurrence of charge transfer mechanism between anthracene part to the imine part of the probe. After the binding of AA with ADD through hydrogen bonding, the charge transfer is occurred between the donor luminol part to acceptor part AA (luminol-AA complex). This may be attributed to the occurrence of FRET type mechanism and it is was further supported by the overlapping of donor emission and acceptor absorbance spectra as given in the graphical and Scheme 1. Hydrogen bond formation between analyte and probe was reported by so many research groups (Astray et al., 2009; Gao et al., 2018; Liu et al., 2018; Xu et al., 2018). The stoichiometry responses for Probe: Analyte was determined by using the Jobs plot. In this case, ADD and AA were fixed at a same concentration of 0.001 M in pH 7.4 buffer and emission intensity was measured. The Jobs plot is drawn in which the mole fraction vs intensity intersects at ~0.5 mol fractions. The stoichiometry binding between ADD: AA is found as 1:1 ratio (Fig. S6) (Ciupa, Mahon, De Bank, & Caggiano, 2012; Hatai, Pal, Jose, & Bandyopadhyay, 2012; Sutariya et al., 2012). The Stern-Volmer quenching constant has also added at additional support for the FRET type of quenching.

Table 2
Comparison of the performance of ADD probe with existing literature for AA detection.

Method	Materials	LOD	Linear Range	Ref.
Fluorescence	GQDs	200 nM	1.0–95 μM	(Gao et al., 2018)
Fluorescence	GQDs	20.3 nM	0–12 μM	(Na et al., 2018)
Fluorescence	4-azide-7-nitrobenzo-2-oxa-1,3 diazole (NBD-N_3)	–	0–100 μM	(Biswas et al., 2018)
Fluorescence	CdSe@SiO_2@CdTe quantum dot hybrid	35 nM	0.1– 5 μM	(Wang, Peng, Li, Jiang, Pan, Chen, et al., 2017)
Fluorescence	BNS-CDs@Fe^{3+}	0.3 μM	1– 600 μM	(Y. Liu, Wei, Duan, Ren, Wu, Liu et al., 2018)
Fluorescence	GQDs	0.32 μM	1.11–300 μM	(Liu et al., 2017)
Fluorescence	Carbon nanocages (CNCs)	97.2 nM	2–12 μM	(Bi, Wang, Kamal, Zhu, & Tan, 2017)
Fluorescence	MoS_2 quantum dots-MnO_2 nanosheets system	39 nM	0.33–5.00 mM	(Xu, Niu, Chen, Zhao, & Chen, e al., 2017)
Fluorescence	Cu-ZnCdS QDs and α-MnO_2 nanorods	31.62 μM	5.02–401.77 μM	(Rao et al., 2017)
Fluorescence	Bimodal action of Nitronyl-Nitroxide	13.6 μM	1 μM–2 mM	(Nam, Kwon, Choi, Seo, Shin, Kim, et al., 2016)
Fluorescence	Carbon dots	20 μg/mL	24–40 μg/mL	(Fong et al., 2016)
Fluorescence	Carbon quantum dots − MnO_2	42 nM	0.18–90 μM	(Liu et al., 2016)
Fluorescence	Profluorescentnitroxideunique radical based redox active	1.8 nM	8.0–100 nM	(Matsuoka, Yamato, & Yamada, et al., 2016)
Fluorescence	E)-5-((anthrcene-9-ylmethylene) amino)-2, 3dihydrophthalazine) 1–4-dione (ADD)	10 nM	0.25–190 μM	This Work

3.8. Real sample analysis

AA rich fruits and vegetables were purchased from local night market at Yongsheng road, yonghe district in Taipei city and they were cleaned with fresh water, further dried in room temperature for 30 mins and cut into small pieces and grinding in phosphate buffer and centrifuged at 5000 rpm (HERMLE-Z 206A) for 10 mins. Then, supernatant solution was filtered using whatman filter paper and then it was diluted for the analysis of AA. A linear plat was prepared drawn between known concentration AA and corresponding emission intensity. The concentrations unknown of real samples were calculated from the above linear plot. Then, the different concentrations of AA were spiked with the sensing solution (at previously optimised condition) and then incubated for 5 mins at RT. The same procedures were followed for remaining real samples. The reproducibility of the real samples were also tested and observed the same results (Fig. S7). The data obtained from the above spectra are given in Table 1. Fig. S7 Based on these results, we conclude that the ADD is acting as a good optical sensing probe for the selective detection of AA in real samples and this analysis could be a potential sensing tool for practical applications. Finally, the analytical performance of optical biosensor was compared with several of previous reported elements probes for AA detection (Table 2).

4. Conclusion

In summary, we have adopted a greener methodology for synthesizing a simple imine based novel fluorescent probe, ADD for the quantitative detection of AA in aqueous neutral medium. The developed simple biosensor has shown a broad linear range of AA from 0.25 to 190 μM along with an excellent LOD of 10 nM. Moreover, the synthesis of ADD involved less time and cost effective. It shows high selectivity sensitivity and competitivity towards AA detection while comparing with other optical sensors reported so far. The real time application of the developed biosensor has demontrated in various food samples like fruits and vegetables directly and the results have shown a very good agreement with our optimized results. Hence, the developed optical biosensor could be act as a very useful sensing platform for AA in practical applications.

CRediT authorship contribution statement

Shenbagavalli Kathiravan: Writing - original draft. **Ellairaja Sundaram:** Review & editing. **Bella Antony Paulraj:** Methodology. **Princy Merlin Johnson:** Methodology. **Sheng-Tung Huang:** Methodology. **Veerappan Mani:** Methodology. **Vairathevar Sivasamy Vasantha:** Conceptualization, Investigation, Supervision.

Declaration of Competing Interest

The authors declare that they have no known competing financial interests or personal relationships that could have appeared to influence the work reported in this paper.

Acknowledgement

Sincere thanks to very helpful supporting for acknowledges DST-SERB funding agency for EMR/2015/002035 [diary No. SERB/F/8689/2015-16 dated March 29, 2016]. Bella AB sincerely acknowledges the Department of Science and Technology (DST), New Delhi, India for the financial support through the DST-WOS-A Project [Ref. No. SR/WOS-A/CS-22/2016].

Appendix A. Supplementary data

Supplementary data to this article can be found online at https://doi.org/10.1016/j.foodchem.2020.127150.

References

Ankireddy, S. R., & Kim, J. (2015). Selective detection of dopamine in the presence of ascorbic acid via fluorescence quenching of InP/ZnS quantum dots. International Journal of Nanomedicine, 10 Spec Iss, 113-119.

Astray, G., Gonzalez-Barreiro, C., Mejuto, J. C., Rial-Otero, R., & Simal-Gándara, J. (2009). A review on the use of cyclodextrins in foods. *Food Hydrocolloids, 23*, 631–1640.

Badea, M., Chiperea, S., Balan, M., Floroian, L., Restani, P., Marty, J. L., et al. (2018). New approaches for electrochemical detection of ascorbic acid. *Farmacia, 66*(1), 83–87.

Bi, J., Wang, H., Kamal, T., Zhu, B.-W., & Tan, M. (2017). A fluorescence turn-off-on chemosensor based on carbon nanocages for detection of ascorbic acid. *RSC Advances, 7*(48), 30481–30487.

Biswas, S., Pal, K., Kumar, P., & Koner, A. L. (2018). A fluorogenic probe for in vitro and in vivo detection of biothiols and vitamin-C with an in-depth mechanistic understanding. *Sensors and Actuators B: Chemical, 256*, 186–194.

Bushway, R. J., King, J. M., Perkins, B., & Krishnan, M. (1988). High-performance liquid chromatographic determination of ascorbic acid in fruits, vegetables and juices. *Journal of Liquid Chromatography, 11*(16), 3415–3423.

Ciupa, A., Mahon, M. F., De Bank, P. A., & Caggiano, L. (2012). Simple pyrazoline and pyrazole "turn on" fluorescent sensors selective for Cd2+ and Zn2+ in MeCN. *Organic and Biomolecular Chemistry, 10*(44), 8753–8757.

Csiff Ary, G., Péter, F., Adanyi, N., & Att ila, K. (2016). Ascorbate oxidase-based amperometric biosensor for L-ascorbic acid determination in beverages. *Food Technology and Biotechnology, 54*(1), 31–35.

Dey, S. K., Al Kobaisi, M., & Bhosale, S. V. (2018). Functionalized quinoxaline for chromogenic and fluorogenic anion sensing. *ChemistryOpen, 7*(12), 934–952.

El-Din, M. S. (2012). Development and validation of RP-HPLC method for simultaneous determination of ascorbic acid and salicylamide in their binary mixtures: Application to combined tablets. *Journal of Chromatography & Separation Techniques, 03*(05).

Elgailani, I. E. H., Elkareem, M. A. M. G., Noh, E. A. A., Adam, O. E. A., & Alghamdi, A. M. A. (2017). Comparison of two methods for the determination of vitamin C (ascorbic acid) in some fruits. *American Journal of Chemistry, 2*(1), 1–7.

Ellairaja, S., Shenbagavalli, K., Ponmariappan, S., & Vasantha, V. S. (2017). A green and facile approach for synthesizing imine to develop optical biosensor for wide range detection of bilirubin in human biofluids. *Biosensors and Bioelectronics, 91*, 82–88.

Fong, J. F. Y., Chin, S. F., & Ng, S. M. (2016). A unique "turn-on" fluorescence signalling strategy for highly specific detection of ascorbic acid using carbon dots as sensing probe. *Biosensors and Bioelectronics, 85*, 844–852.

Gai, P., Zhang, H., Zhang, Y., Liu, W., Zhu, G., Zhang, X., & Chen, J. (2013). Simultaneous electrochemical detection of ascorbic acid, dopamine and uric acid based on nitrogen doped porous carbon nanopolyhedra. *Journal of Materials Chemistry B, 1*(21), 2742.

Gao, Y., Yan, X., Li, M., Gao, H., Sun, J., Zhu, S., et al. (2018). A "turn-on" fluorescence sensor for ascorbic acid based on graphene quantum dots via fluorescence resonance energy transfer. *Analytical Methods, 10*(6), 611–616.

Girigoswami, K., & Akhtar, N. (2019). Nanobiosensors and fluorescence based biosensors: An overview. *International Journal of Nano Dimension, 10*(1), 1–17.

Gualandi, A., Savoini, A., Saporetti, R., Franchi, P., Lucarini, M., & Cozzi, P. G. (2018). A facile hydroxylation of arylboronic acids mediated by sodium ascorbate. *Organic Chemistry Frontiers, 5*(10), 1573–1578.

Hasanin, T. H. A., & Fujiwara, T. (2018). Flow-injection chemiluminescence method for sensitive determination of ascorbic acid in fruit juices and pharmaceutical samples using a luminol-cetyltrimethylammonium chloride reversed micelle system. *Analytical Sciences, 34*(7), 777–782.

Hatai, J., Pal, S., Jose, G. P., & Bandyopadhyay, S. (2012). Histidine based fluorescence sensor detects Hg2+ in solution, paper strips, and in cells. *Inorganic Chemistry, 51*(19), 10129–10135.

He, B. S., & Zhang, J. X. (2017). Rapid detection of ascorbic acid based on a dual-electrode sensor system using a powder microelectrode embedded with carboxyl multi-walled carbon nanotubes. *Sensors (Basel), 17*(7).

He, D., Li, S., Zhang, P., & Luo, H. (2017). CVD graphene incorporating polymerized l-cysteine as an electrochemical sensing platform for simultaneous determination of dopamine and ascorbic acid. *Analytical Methods, 9*(47), 6689–6697.

Klos-Witkowska, A. (2016). The phenomenon of fluorescence in immunosensors. *Acta Biochimica Polonica, 63*(2), 215–221.

Liu, H., Na, W., Liu, Z., Chen, X., & Su, X. (2017). A novel turn-on fluorescent strategy for sensing ascorbic acid using graphene quantum dots as fluorescent probe. *Biosensors and Bioelectronics, 92*, 229–233.

Liu, J., Chen, Y., Wang, W., Feng, J., Liang, M., Ma, S., & Chen, X. (2016). "Switch-on" fluorescent sensing of ascorbic acid in food samples based on carbon quantum dots-MnO2 probe. *Journal of Agricultural and Food Chemistry, 64*(1), 371–380.

Liu, S., & Pang, S. (2018). A dual-model strategy for fluorometric determination of ascorbic acid and of ascorbic acid oxidase activity by using DNA-templated gold-silver nanoclusters. *Microchimica Acta, 185*(9), 426.

Liu, X., Ou, X., Lu, Q., Zhang, J., Chen, S., & Wei, S. (2014). Electrochemical sensor based on overoxidized dopamine polymer and 3,4,9,10-perylenetetracarboxylic acid for simultaneous determination of ascorbic acid, dopamine, uric acid, xanthine and hypoxanthine. *RSC Advances, 4*(80), 42632–42637.

Liu, Y., Wei, Z., Duan, W., Ren, C., Wu, J., Liu, D., & Chen, H. (2018). A dual-mode sensor for colorimetric and "turn-on" fluorescent detection of ascorbic acid. *Dyes and Pigments, 149*, 491–497.

Matsuoka, Y., Yamato, M., & Yamada, K. (2016). Fluorescence probe for the convenient and sensitive detection of ascorbic acid. *J Clin Biochem Nutr, 58*(1), 16–22.

M.J, F., G.W, T., B, S. H., E, S. G., M.A., R., R, C. J., G, S., V, B., B, M., & A, P. G. (2010). Gaussian 09, Revision B.01.

Na, W., Qu, Z., Chen, X., & Su, X. (2018). A turn-on fluorescent probe for sensitive detection of sulfide anions and ascorbic acid by using sulfanilic acid and glutathione functionalized graphene quantum dots. *Sensors and Actuators B: Chemical, 256*, 48–54.

Rao, H., Gao, Y., Ge, H., Zhang, Z., Liu, X., Yang, Y., et al. (2017). An "on-off-on" fluorescent probe for ascorbic acid based on Cu-ZnCdS quantum dots and alpha-MnO2 nanorods. *Analytical and Bioanalytical Chemistry, 409*(19), 4517–4528.

Su, C. H., Sun, C. L., & Liao, Y. C. (2017). Printed combinatorial sensors for simultaneous detection of ascorbic acid, uric acid, dopamine, and nitrite. *ACS Omega, 2*(8), 4245–4252.

Sutariya, P. G., Modi, N. R., Pandya, A., Joshi, B. K., Joshi, K. V., & Menon, S. K. (2012). An ICT based "turn on/off" quinoline armed calix[4]arene fluoroionophore: Its sensing efficiency towards fluoride from waste water and Zn2+ from blood serum. *Analyst, 137*(23), 5491–5494.

Tortajada-Genaro, L. A. (2012). Determination of l-ascorbic acid in tomato by capillary electrophoresis. *Journal of Chemical Education, 89*(9), 1194–1197.

Tukimin, N., Abdullah, J., & Sulaiman, Y. (2018). Review—Electrochemical detection of uric acid, dopamine and ascorbic acid. *Journal of the Electrochemical Society, 165*(7), B258–B267.

Wang, H., Pu, G., Devaramani, S., Wang, Y., Yang, Z., Li, L., et al. (2018). Bimodal electrochemiluminescence of G-CNQDs in the presence of double coreactants for ascorbic acid detection. *Analytical Chemistry, 90*(7), 4871–4877.

Wu, D., Sedgwick, A. C., Gunnlaugsson, T., Akkaya, E. U., Yoon, J., & James, T. D. (2017). Fluorescent chemosensors: The past, present and future. *Chemical Society Reviews, 46*(23), 7105–7123.

Xu, H., Cai, Q., Nie, Q., Qiao, Z., Liu, S., & Li, Z. (2018). Ultrasensitive determination of ascorbic acid by using cobalt oxyhydroxide nanosheets to enhance the chemiluminescence of the luminol–H_2O_2 system. *RSC Advances, 8*(42), 23720–23726.

Xu, Y.-L., Niu, X.-Y., Chen, H.-L., Zhao, S.-G., & Chen, X.-G. (2017). Switch-on fluorescence sensor for ascorbic acid detection based on MoS 2 quantum dots-MnO 2 nanosheets system and its application in fruit samples. *Chinese Chemical Letters, 28*(2), 338–344.

Zhang, L., Wang, G., Wu, D., Xiong, C., Zheng, L., Ding, Y., et al. (2018). Highly selective and sensitive sensor based on an organic electrochemical transistor for the detection of ascorbic acid. *Biosensors and Bioelectronics, 100*, 235–241.

Zhang, Q., Wang, C. F., & Lv, Y. K. (2018). Luminescent switch sensors for the detection of biomolecules based on metal-organic frameworks. *Analyst, 143*(18), 4221–4229.

Zhu, H. (2017). Electrochemical determination of ascorbic acid based on hydrothermal synthesized ZnO nanoparticles. *International Journal of Electrochemical Science,* 3873–3882.

Zhu, Q., Dong, D., Zheng, X., Song, H., Zhao, X., Chen, H., & Chen, X. (2016). Chemiluminescence determination of ascorbic acid using graphene oxide@copper-based metal–organic frameworks as a catalyst. *RSC Advances, 6*(30), 25047–25055.